PLOS NEGLECTED TROPICAL DISEASES

RESEARCH ARTICLE

Identifying and validating the presence of Guanine-Quadruplexes (G4) within the blood fluke parasite *Schistosoma mansoni*

Holly M. Craven[1], Riccardo Bonsignore[2], Vasilis Lenis[3], Nicolo Santi[4], Daniel Berrar[5], Martin Swain[1], Helen Whiteland[1], Angela Casini[2], Karl F. Hoffmann[1]*

1 Institute of Biological, Environmental and Rural Sciences (IBERS), Aberystwyth University, United Kingdom, **2** Department of Chemistry, Technical University of Munich, Germany, **3** School of Health and Life Sciences, Teesside University, United Kingdom, **4** School of Chemistry, Cardiff University, Cardiff, United Kingdom, **5** Data Science Laboratory, Tokyo Institute of Technology, Tokyo, Japan

* krh@aber.ac.uk

Citation: Craven HM, Bonsignore R, Lenis V, Santi N, Berrar D, Swain M, et al. (2021) Identifying and validating the presence of Guanine-Quadruplexes (G4) within the blood fluke parasite *Schistosoma mansoni*. PLoS Negl Trop Dis 15(2): e0008770. https://doi.org/10.1371/journal.pntd.0008770

Editor: Neil David Young, The University of Melbourne, AUSTRALIA

Received: September 2, 2020

Accepted: February 2, 2021

Published: February 18, 2021

Data Availability Statement: All relevant data are within the manuscript and its Supporting Information files.

Funding: This research was funded in whole, or in part, by the Wellcome Trust [Grant number 107475/Z/15/Z]. For the purpose of Open Access, the author has applied a CC BY public copyright licence to any Author Accepted Manuscript version arising from this submission. The work was additionally funded by Aberystwyth University

Abstract

Schistosomiasis is a neglected tropical disease that currently affects over 250 million individuals worldwide. In the absence of an immunoprophylactic vaccine and the recognition that mono-chemotherapeutic control of schistosomiasis by praziquantel has limitations, new strategies for managing disease burden are urgently needed. A better understanding of schistosome biology could identify previously undocumented areas suitable for the development of novel interventions. Here, for the first time, we detail the presence of G-quadruplexes (G4) and putative quadruplex forming sequences (PQS) within the *Schistosoma mansoni* genome. We find that G4 are present in both intragenic and intergenic regions of the seven autosomes as well as the sex-defining allosome pair. Amongst intragenic regions, G4 are particularly enriched in 3´ UTR regions. Gene Ontology (GO) term analysis evidenced significant G4 enrichment in the *wnt* signalling pathway ($p<0.05$) and PQS oligonucleotides synthetically derived from *wnt*-related genes resolve into parallel and anti-parallel G4 motifs as elucidated by circular dichroism (CD) spectroscopy. Finally, utilising a single chain anti-G4 antibody called BG4, we confirm the *in situ* presence of G4 within both adult female and male worm nuclei. These results collectively suggest that G4-targeted compounds could be tested as novel anthelmintic agents and highlights the possibility that G4-stabilizing molecules could be progressed as candidates for the treatment of schistosomiasis.

Author summary

Schistosoma mansoni causes schistosomiasis, a parasitic disease that affects millions of people living in resource-deprived areas of developing countries. No vaccine exists and the current drug treatment has limitations, notably inefficacy against the larval stages of the parasite. New drugs are, therefore, needed to sustainably control schistosomiasis. A

(https://www.aber.ac.uk/en/) and the Joy Welch Educational Charitable Trust.

Competing interests: The authors have declared that no competing interests exist.

further understanding of parasite biology will uncover new targets and lead to the development of novel therapies. Here, we identify the presence of G-Quadruplexes (G4s) in *S. mansoni*. G4s are four-stranded DNA structures that can affect gene function and, to date, have not been previously found in any parasitic helminth. Computational analysis predicted potential G4 folding sequences within the *S. mansoni* genome, several of which were confirmed to fold by circular dichroism spectroscopy. Analysis of G4-containing protein coding genes found an enrichment within the *wnt* signalling pathway, a developmental pathway crucial for axial development in the parasite. Additionally, G4s could be detected within adult worms using a fluorescent antibody that selectively recognises quadruplex structures in nucleic acids. This research describes the presence of a previously unknown structure within the parasite, which could present a new target for developing novel treatments.

Introduction

Schistosoma mansoni, a digenean platyhelminth responsible for the neglected tropical disease (NTD) schistosomiasis, maintains its complex lifecycle through definitive human and intermediate snail (*Biomphalaria sp.)* hosts. Exhibiting dioecy as adults, mature *S. mansoni* pairs establish infection within the human mesenteric vessels draining the intestine. While adults are largely non-immunogenic, copulation between schistosome pairs leads to the production of an estimated 300 immunogenic eggs per day. Approximately half of these eggs migrate through the mesenteric veins and reach the intestinal lumen where they are released with faeces, a requirement for lifecycle transmission. Endemic in sub-tropical regions both in the new and old world, schistosomiasis contributes to socioeconomic developmental arrest and is a public health burden in many developing countries. It is estimated that some 250 million individuals worldwide suffer from schistosomiasis per annum, with the disease accounting for the loss of 2.5 million DALYs (disability adjusted life years) in 2016 [1].

The *S. mansoni* genome, first published in 2009 [2], updated in 2012 [3] and under continual refinement in WormBase-Parasite (current assembly version 7) has facilitated the advancement of many basic investigations of schistosome biology [4–8]. However, much of what powers survival and developmental success within the parasite remains unknown. It is, therefore, vital that research identifying vulnerabilities in the schistosome genome continues to facilitate development of new schistosomiasis control strategies in light of existing limitations associated with praziquantel mono-chemotherapy [9, 10].

Guanine quadruplexes (G4s) have recently been implicated as targets for the control of both infectious diseases (caused by *Plasmodium*, *Leishmania* and *Trypanosoma* species) and noncommunicable diseases (notably in solid cancers) [11–16]. Found to be evolutionarily conserved across phyla (eukaryotes, prokaryotes, viruses), these four stranded DNA and RNA structures fold from guanine (G) rich regions in the genome [17–21]. Guanines form planar tetrads mediated through Hoogsteen hydrogen bonds internally stabilised by monovalent cations, usually K^+ [22]. These tetrads stack and arrange into a tertiary structure known as a quadruplex, joined by intermediate loops formed of any other nucleobase (i.e. cytosine, adenine, guanine, thymine or uracil). While G4s are less stable than duplex DNA and are frequently found in single stranded telomeric overhangs, upstream promoter regions or within genes, their transient formation at these positions can directly affect transcription, translation and replication [23–25]. Approximately 50% of all human genes are predicted to contain a G4 within or near promotor regions [26] as well as in 5′ UTRs [21].

In *P. falciparum*, a species with a particularly AT rich genome, putative quadruplex forming sequences (PQS) are found within VAR genes as well as in telomeric regions [11, 15, 18]. In *T. brucei*, a main G4 sequence of interest is a highly repeated 29 nucleotide long PQS (referred to as EBR1; Efres Belmonte-Reche-1) which exhibits selective binding to G4 ligand carbohydrate naphthalene diimide derivatives when compared to dsDNA. These ligands were shown to have antiparasitic activity, indicating G4 targeting could be a potential therapeutic avenue [27]. Nevertheless, to our knowledge there have been no in-depth investigations into the presence of G4s within extracellular endoparasites such as those species contained within the Platyhelminthes. As *S. mansoni* possesses a more GC rich genome than *P. falciparum* (~34% compared to ~18% respectively) [3, 28], this suggests that PQS could be present. Moreover, similar to *P. falciparum*, *S. mansoni* contains a TTAGGG telomeric tandem repeat, which, in humans, has been demonstrated to fold into G4 and is linked with telomere capping [29]. The discovery of G4s within the schistosome genome could, therefore, identify a new molecular regulator of biological processes and genome architecture. In turn, G4-targetting compounds could modulate these activities and structures, ultimately leading to the development of novel strategies for controlling a major NTD. Here, we present the first description of PQS within *S. mansoni* that will foster further investigations in this promising area.

Materials and methods

Ethics statement

All procedures performed on mice adhered to the United Kingdom Home Office Animals (Scientific Procedures) Act of 1986 (project licenses PPL 40/3700 and P3B8C46FD) as well as the European Union Animals Directive 2010/63/EU and were approved by Aberystwyth University's (AU) Animal Welfare and Ethical Review Body (AWERB).

Genome preparation

FASTA files of the *S. mansoni* genome (version 7.1) used for computational analyses of PQS were obtained from the Wellcome Sanger Institute [30]. Scaffolds not assigned to the chromosome assembly were not used. Gene annotations, obtained from the associated general feature format (GFF) extension files, were used to assign PQS to intragenic regions including CDS (coding sequence), five prime UTR (5′ UTR) and three prime UTR (3′ UTR) as defined from the annotation GFF file. Intronic regions were not labelled within the GFF and were calculated by extracting the regions between exons using in house scripts. All other annotation types were excluded.

Quadparser (QP) analysis of genome

QP [31] was compiled in Linux. Genome FASTA files were run through QP using parameters $G_{3+}N_{1-7}G_{3+}N_{1-7}G_{3+}N_{1-7}G_{3+}$ and $C_{3+}N_{1-7}C_{3+}N_{1-7}C_{3+}N_{1-7}C_{3+}$ where G = guanine, C = cytosine and N = A, T, C or G. This allows G4s present on both the forward and reverse strand to be detected. Output of PQS were formatted into a browser extensible data (.BED) format file for visualisation with the Integrative Genomics Viewer (IGV) v2.4.2 desktop application [32].

G4Hunter (G4h) analysis of genome

G4h [33] was executed through a Bourne-again shell (Bash) environment. Genome FASTA were run through G4h using a fixed nucleotide window of 30 and a score threshold of ±1.4. Positive scores indicate G4 on the forward strand, and negative scores indicate G4 on the reverse strand.

PQS overlap, normalisation and density quantification

The Bedtools package [34] was used to find overlapping PQS in both QP and G4h outputs. These commonly identified loci were then further defined by intragenic occurrences (present in CDS, 5′ UTR, 3′ UTR and intron GFF notations). Bedtools was subsequently used to acquire *S. mansoni* protein coding genes (Smps) containing intragenic PQS. Further Smp data were extracted using the WormBase Parasite Biomart function as well as the scientific literature [2, 3, 35, 36]. PQS density was calculated as the number of PQS per chromosome per Mb of feature/chromosome. A baseline of total PQS density per genome length was calculated to identify over or under enrichment of PQS within intragenic features on different chromosomes. Analysis of enrichment was performed by calculating PQS/Mb densities. The significance of the differences was assessed by χ^2 test in R [37]. The *p* values were corrected for multiple testing with the Bonferroni-Holm method [38].

Gene Ontology (GO) classification

GOAtools analysis scripts [39] were used to quantify functional groupings within the PQS-containing Smps; a *p* value cut-off of 0.05 was selected to identify statistically significant terms. Genes were listed only once regardless of the number of PQS contained within them.

Circular Dichroism (CD) spectroscopy

DNA oligonucleotides (Table 1) for CD analysis were obtained from Eurogentec (Belgium), supplied at 1000 nmol scale, RP-HPLC purified, desalted and reconstituted to 100 μM in biological grade water (VWR, US). Oligos were adjusted to a 6 μM working solution in either 60 mM TrisKCl (10 mM TrisHCl, 50 mM KCl; pH 7.4) or 10 mM TrisHCl (pH 7.4) buffers. Oligos were denatured for 5 min at 95˚C in an oil bath and left to cool to room temperature (RT) prior to analysis. Spectra were recorded on a Chirascan (Applied Photophysics, UK) CD spectrometer measuring between 210–400 nm at 25˚C, step 1 nm. Triplicate reads were performed, and traces averaged and smoothed. A 60 mM TrisKCl (pH 7.4) or a 10 mM TrisHCl (pH 7.4) buffer only background were additionally run, and baseline subtracted from each respective read. For G4-melting assays, the oligonucleotide concentrations were adjusted to 6 μM in 60 mM TrisKCl (pH 7.4) buffer. Spectra were recorded as defined above, with a 5˚C ramp from 25˚C to 95˚C with a 2 min equilibration hold prior to reading.

S. mansoni adult worm cultures

Female HsdOla:TO mice (ENVIGO, UK) were infected with 180 cercariae via percutaneous exposure for 40 min. Adult worms were perfused 7 wk post infection as described previously

Table 1. Genomic identifiers and oligonucleotide sequences used in CD spectroscopy.

Gene ID	Name	Oligonucleotide Sequence for CD Analysis (5′- 3′)
Smp_196840	Collagen α 1 chain	GGGAGGGGGAGAGAGAGAGGGGGAGGTAAAGGG
Smp_139180	Frizzled (Fzd)	GGGCGAAACGGGGCAGCAAGGGCAGAGAGGGGCTCCTGGG
Smp_127680	Rabconnectin Related	GGGTAAAGGAGGGTTGGGCATGGGG
Smp_145140	Wingless (Wnt)	GGGTAACTGAGGGTTGGGCATGGGG
Smp_319480	Myb like protein V	GGGGGAGAGAGAGGGAGAGAGGGAGGG
Smp_163240	Tbx2	GGGTGGGTGTGGGTGGGAGGG
SmTelo tandem repeat *	Telomeric tandem repeat	GGGTTAGGGTTAGGGTTAGGG
c-myc	C-myc	GGGAGGGTGGGGAGGGTGGG

* Represents the recurring (repeat) sequence found on all Sm chromosome termini [29]

https://doi.org/10.1371/journal.pntd.0008770.t001

[40, 41]. Parasites were cultured for 24 hrs at a density of three worm pairs per well in a 48 well tissue culture plate (Fischer Scientific, UK) in 1 mL of complete media (DMEM, 1% Penicillin-Streptomycin, 200 mM L-glutamine, 10% FBS, 10% HEPES) at 37˚C in a humidified environment containing 5% CO_2.

In situ detection of G4s in schistosomes

Cultured 7 wk adult schistosomes were incubated in a 0.25% (w/v) solution of the anaesthetic ethyl 3-aminobenzoate methanesulfonate in complete media for 10 min before being killed in a 0.6 M $MgCl_2$ solution. Worms were subsequently fixed overnight in ice cold 3:1 methanol: acetic acid at -20˚C prior to 1 hr permeabilisation in PBS containing 0.3% (v/v) Triton X-100 (PBSTx) at RT. Following permeabilisation, schistosomes were blocked for 2 hrs at RT in blocking buffer (5% BSA (w/v) in PBSTx) and then incubated for 72 hrs at 4˚C in 1:400 anti-RNA/DNA G-Quadruplex antibody BG4 (Ab00174-10.6, Absolute Antibody, Oxford UK) diluted in blocking buffer. Parasites were washed thrice for 15 min in PBSTx and incubated for 24 hrs in 1:2000 F_{ab} specific FITC conjugated goat anti human IgG (F5512, Sigma-Aldrich UK) diluted in blocking buffer. Samples were washed again with PBSTx and mounted on microscope slides in Vectashield anti-fade mounting medium counterstained with 5 μg/mL DAPI. Negative controls were incubated in either 120 U DNase I or 0.1 mg/mL RNase A in PBS for 1 hour at 37˚C 5% CO_2 in a humidified environment post permeabilisation. Slides were imaged on a Leica TCS SP8 Laser Confocal Scanning Microscope at x20 air or x100 oil immersion at 8000 Hz, using DPSS and Argon laser intensities at 20%. Anterior, midsection and posterior images were collated from 100 Z stacks and representative images taken from each group (n = 8) are shown. RNase was tested by incubation of 0.1 mg/mL RNase A with 1 μM of either universal mouse RNA (QS0640, ThermoFisher UK) or extracted *S. mansoni* RNA [42] for 1 hour at 37˚C. The digested RNA was then electrophoresed on a 1% agarose gel in TAE buffer at 8 V/cm and visualised using a UVP Gel Doc-it.

Results

The *S. mansoni* genome was searched for the presence of G4 using two different algorithms, quadparser (QP) and G4Hunter (G4h). PQS-containing loci identified by both algorithms were retrieved and used to compile a high stringency list of overlapping genomic positions (n = 406) (Fig 1 and S1 Table). While high stringency searches will result in fewer returned sequences, they have the greatest likelihood of folding the canonical intramolecular G4 *in vivo*. Here, high stringency selected PQS were found unequally distributed across both intragenic (n = 122) and intergenic (n = 284) regions.

Global distribution of these selected 406 high stringency PQS (both intragenic and intergenic) across the *S. mansoni* genome was first assessed (Fig 2). Initial observations indicated that PQS were found within all seven autosomes as well as the sex-defining allosome ZW pair, with numerous PQS appearing towards the ends of chromosomes (Fig 2A). Furthermore, PQS were identified on both forward and reverse strands as well as at chromosomal termini in the form of TTAGGG tandem telomeric repeats on all chromosomes (Fig 2B and S2 Table) [29]. The largest total number of PQS was found on chromosome 5 (n = 100) and the smallest number was found on chromosome 7 (n = 19) (Fig 2C and Table 2).

To test if PQS are randomly distributed or are enriched in particular chromosomes, PQS per Mb were calculated for each chromosome and compared to a baseline (average of 1.03 PQS per Mb found in the complete chromosomal assembly, Fig 2D). Data points above the baseline can be considered enriched in PQS (Fig 2D and Table 3). Accordingly, four *S. mansoni* chromosomes (chromosomes 2, 3, 5 and 6) are enriched for PQS when compared to the

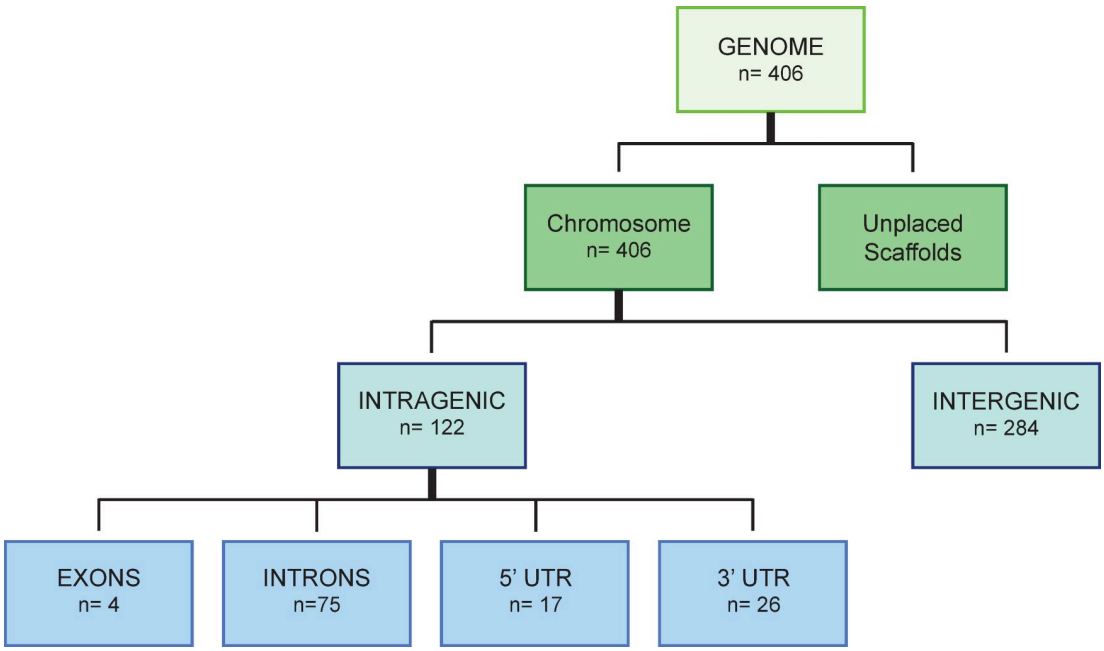

Fig 1. Flowchart for identifying PQS found in the *S. mansoni* genome. Quadparser and G4Hunter were used to independently identify PGS within the *S. mansoni* genome (v7.1). The Bedtools intersect function was subsequently used to find overlapping PQS detected by both methods. Across the assembled chromosome scaffolds (genome), this led to the discovery of 406 PQS. Unplaced scaffolds were not included in the analysis. Intragenic PQS analysis, determined using the genome annotation file, found 122 of these to be within either Exons (4), Introns (75), 5′ UTRs (17) or 3′ UTRs (26). Those PQS deemed intergenic are found within chromosomes but not within intragenic regions.

https://doi.org/10.1371/journal.pntd.0008770.g001

baseline frequency detected across the whole genome, with chromosome 5 particularly enriched. Chromosomes 1, 4, 7 and ZW were considered unenriched for PQS by this analysis. After adjusting for chromosome size, we used χ^2 test to assess the PQS distribution across normalised chromosomes and observed a significant difference ($p < 2.2x10^{-16}$). We then carried out all pair-wise comparisons using the Bonferroni-Holm method to adjust for multiple testing. We found that chromosome 5 had a greater density of total PQS, compared to any other chromosome (3.96 PQS/Mb). Given chromosome 5 is a relatively short chromosome (25 Mb), this indicated that the presence of PQS is not solely driven by chromosome length and enrichment may be driven by specific chromosome features, such as intragenic motifs. While chromosome 7 previously had the smallest number of identifiable PQS (n = 19; Table 2), when chromosome length was normalised (PQS/mBase), chromosome 1 contained the lowest density of PQS (0.55 PQS/mBase; Table 3). The effect of chromosome GC content on total and intragenic PQS content was assessed by regression analysis and found to have no association ($R^2 = 0.14$ for total PQS and $R^2 = 0.29$ for Intragenic PQS).

We reasoned that a more thorough interrogation of PQS found only within intragenic regions would generate further clues for interpreting PQS function in the *S. mansoni* genome. Therefore, PQS were next classified according to their location within intragenic features (defined here as 5′- UTR, 3′- UTR, Exon and Intron) of annotated Smps (Figs 1 and 3; Table 2). Analysis of these features concluded that 30% of the 406 PQS found within the *S. mansoni* genome were located within genes (n = 122) with most found in the introns (n = 75) and fewest found in exons (n = 4; Figs 1 and 3A). Furthermore, this analysis indicated that distribution of PQS across intragenic features is not equal: chromosome ZW had the highest number of intragenic PQS (n = 23) and chromosome 7 contained the fewest PQS (n = 7). We

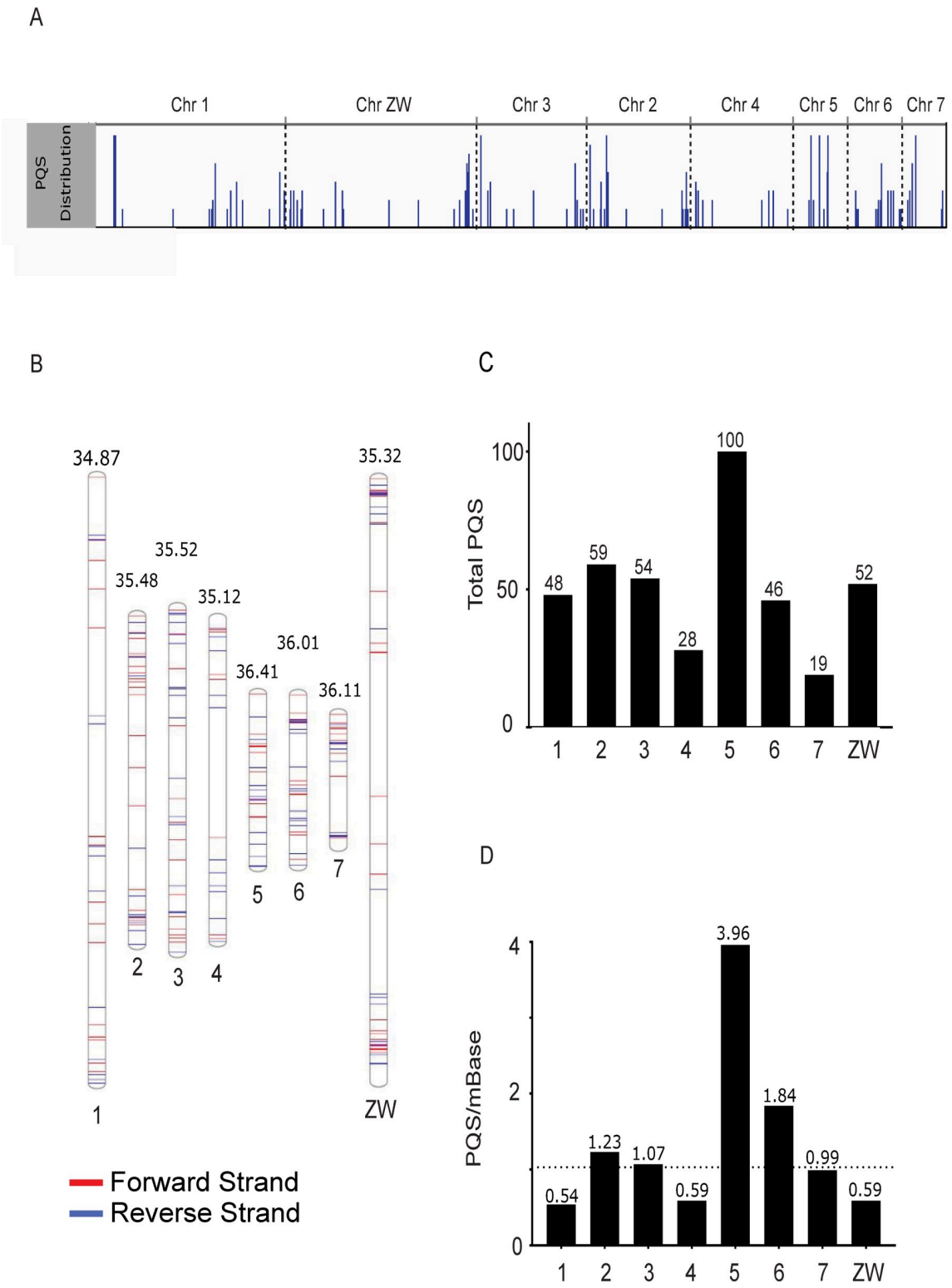

Fig 2. The distribution of PQS across the *S. mansoni* chromosomal assembly. Both intragenic and intergenic PQS (n = 406) were mapped to chromosomes (*S. mansoni* genome, v7.1). A) IGV snapshot of the chromosomal assembly, where PQS appearing in close proximity are visualised as longer bars. Chromosomes are ordered according to size (largest to smallest). B) A phenogram mapping the position of PQS along the length of the chromosome (autosomes ordered sequentially). PQS appear on both forward and reverse strands. Numbers above each chromosome represent % GC content. C) Total number of PQS identified per chromosome (sequentially

ordered). Chromosome 5 has the greatest number of PQS (n = 100) whilst the fewest were detected in chromosome 7 (n = 19). D) PQS density per Mb of chromosome. Average PQS/Mb found in the complete chromosomal assembly is indicated by a dashed line and denotes a baseline. Enrichment of PQS within any chromosome is found above this dotted line.

https://doi.org/10.1371/journal.pntd.0008770.g002

observed a significant difference in the density distribution of PQS across the four intragenic regions ($p = 3.73x10^{-9}$, χ^2 test), with the highest density of 1.76 PQS per Mb found on 3′ UTR. By contrast, exons had the lowest density, with 0.23 PQS per Mb (Fig 3B and Table 3). A post-hoc pair-wise comparison with Bonferroni-Holm correction for multiple testing revealed that, relative to the size of the intragenic regions, there were significantly more PQS found on 3′—UTR compared to 5′- UTR (p = 0.0029), exon ($p = 9.3x10^{-5}$) and intron ($p = 2.6x10^{-8}$) features.

PQS distribution across features was further evaluated at the chromosome level to identify where each of the intragenic PQS were located (Fig 3C and Table 3). Here, intragenic PQS were found broadly distributed across each of the chromosomes. GO term enrichment analysis was subsequently performed on all unique Smps (i.e. some Smps contained more than one PQS) containing PQS (n = 106) using GOAtools [39]; the most significant enrichments were found in GO terms 0016055 (*wnt* signalling pathway) and 1905114 (cell signalling; ($p < 0.00002$; S3 Table).

Following genome analysis, several PQS-containing Smps (Table 1) were selected for circular dichroism (CD) spectroscopy to investigate their folding *in vitro* [43, 44]. Smps were selected such that PQS predicted in all intragenic features were represented: Exon (*smp_196840*); Intron (*smp_1276840*, *smp_145140*); 5′ UTR (*smp_139180* and *smp_319480*); and 3′ UTR (*smp_163240*). The PQS sequences selected also included those with single nucleotide loops (*smp_163240*, *smp_127680* and *smp_319480*) to those with longer loop passages (*smp_196840*; $n \leq 9$). A GO identified enrichment of PQS in *wnt* signalling associated genes meant several wnt associated PQS (*smp_139180*, *smp_145140* and smp_*163240*) were also selected. As different G4 can fold into different topographies (parallel, anti-parallel and hybrid; S1 Fig), controls were selected based on topography. An oligonucleotide representing *H. sapiens c-myc* was utilised as a control for the formation of G4 parallel folding (S1A Fig) [45]. Finally, an oligonucleotide representing *smTelo* was further selected as a control for G4 hybrid folding (S1C Fig), as it contains an identical sequence to the well-studied *H. sapiens* tandem telomeric motif TTAGGG (herein referred to as *hTelo*) located at chromosome termini found to adopt this particular G4 structure [46].

Table 2. PQS numbers and locations within each *S. mansoni* chromosome.

Chromosome	Total Number of PQS and Location Within Each Chromosome					
	All PQS	All intragenic PQS	Intragenic PQS			
			Exon	5′ UTR	3′ UTR	Intron
1	48	19	2	3	2	12
2	59	20	0	4	2	14
3	54	15	1	4	3	7
4	28	11	1	2	1	7
5	100	12	0	0	6	6
6	46	15	0	1	4	10
7	19	7	0	0	3	4
ZW	52	23	0	3	5	15
Total	406	122	4	17	26	75

https://doi.org/10.1371/journal.pntd.0008770.t002

Table 3. PQS density characteristics (PQS/Mb) within each *S. mansoni* chromosome.

Chromosome	PQS per Mb of feature length						
	Chr Length (Mb)	All PQS	All Intragenic PQS	Intragenic			
				Exon	5′ UTR	3′ UTR	Intron
1	88.9	0.55	0.37	0.48	0.44	0.54	0.33
2	48.1	1.23	0.76	0	1.22	1.23	0.73
3	50.5	1.07	0.58	0.46	1.22	1.64	0.38
4	47.3	0.59	0.43	0.48	0.56	0.62	0.38
5	25.3	3.96	1.01	0	0	7.69	0.68
6	25.0	1.84	1.08	0	0.54	4.49	0.99
7	19.3	0.99	0.6	0	0	4.23	0.45
ZW	88.4	0.59	0.44	0	0.44	1.27	0.41
Baseline	-	1.03	0.56	0.23	0.60	1.73	0.48

https://doi.org/10.1371/journal.pntd.0008770.t003

In the presence of K^+, five (*smp_139180*, *smp_145140 smp_163240*, *smp_319480*, *smp_127680*) of the six PQS-containing oligonucleotides selected showed CD spectra compatible with G4-folding (Fig 4). When compared with the *c-myc* G4 sequence, the spectra of *smp_139180 (frizzled)*, *smp_145140 (wnt)* and *smp_163240 (tbx2)* all produced traces with the same positive peaks (between 262 nm– 263 nm) and negative troughs (between 241 nm– 242 nm) characteristic of a parallel G4 structure (Fig 4A). PQS found in *smp_319480* (*myb like protein*) and *smp_127680* (*rab connectin*) displayed a positive peak at 263 nm, a negative peak at 238 nm and a shoulder at 293 nm, mirroring the spectra observed for *smTelo* (a negative peak at 238 nm, shoulder peak at 263 nm and positive peak at 293 nm; Fig 4B) [43, 47]. Based on previously reported results by Karsisiotis and coworkers, investigating the *Giardia* telomeric sequence (pdb id: 2KOW) in K^+ buffer [43], we have attributed these particular CD profiles to the presence of an anti-parallel G4 structure. In contrast, the CD spectrum of the PQS identified in *smp_196840 (collagen α 1 chain)* could not be associated with any known G4-CD profiles, leading us to exclude its folding into any G4 structure in the applied experimental conditions (Fig 4C).

Subsequently, melt curves (from 25˚C to 95˚C) were generated for each of the PQS containing oligonucleotide sequences, in the presence of K^+, to assess structural stability (S2 Fig) and the temperature for which half of the initial ellipticity was lost (melting temperature, T_m) was calculated (S3 Fig). Out of the five tested G4 structures, the oligonucleotide containing the PQS within *smp_145140*, harbouring a parallel G4 conformation, proved to be the most stable as it was not completely melted at 95˚C (S2B Fig). Interestingly, only *smp_319480's* representative oligonucleotide underwent a total loss of ellipticity (S2E Fig) while, even at 95˚C, the other PQSs retained a noticeable secondary structure. Whilst the sequences *smp_139180* (S3A Fig), *smp_127680* (S3D Fig) and *smp_319480* (S3E Fig) share a similar stability ($T_m \approx 60$˚C), the parallel G4 from *smp_163240* (S3C Fig) displayed marked higher stability having a T_m of ca. 80˚C.

To assess the role of a cation for proper folding [47], oligonucleotides containing G4 sequences were annealed in the absence of K^+ and compared to those achieved in presence of 50 mM K^+ (Fig 5). Interestingly, these CD spectra showed differences in folding profiles and ellipticity in all cases, not corresponding to any type of G4-folding. Overall, in the absence of K^+, a large decrease in ellipticity as well as a slight blue shift towards lower wavelengths was observed in all spectra.

Although CD analyses of 5/6 PQS containing oligonucleotides validated the bioinformatics predictions that G4 structures can be formed within the *S. mansoni* genome and fold into

A

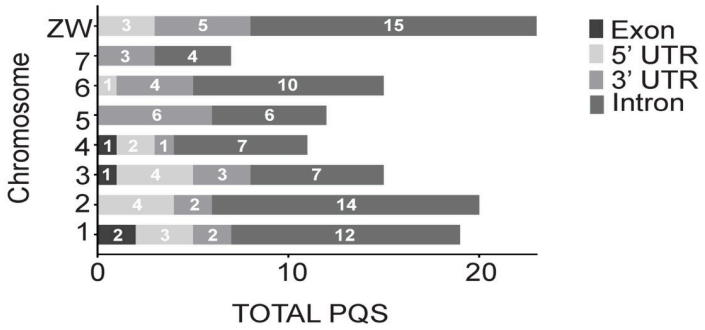
ZW
7
6
5
4
3
2
1
Chromosome
0
10
20
TOTAL PQS
Exon
5' UTR
3' UTR
Intron

B

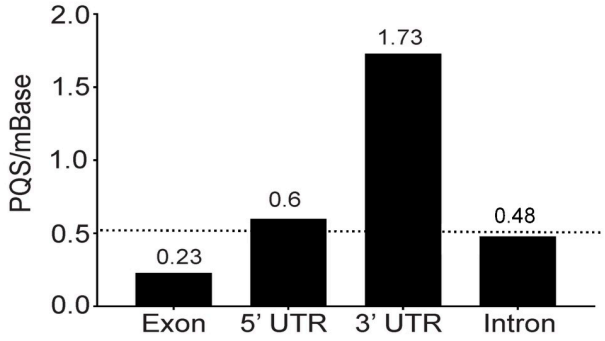
PQS/mBase
2.0
1.5
1.0
0.5
0.0
0.23
0.6
1.73
0.48
Exon
5' UTR
3' UTR
Intron

C

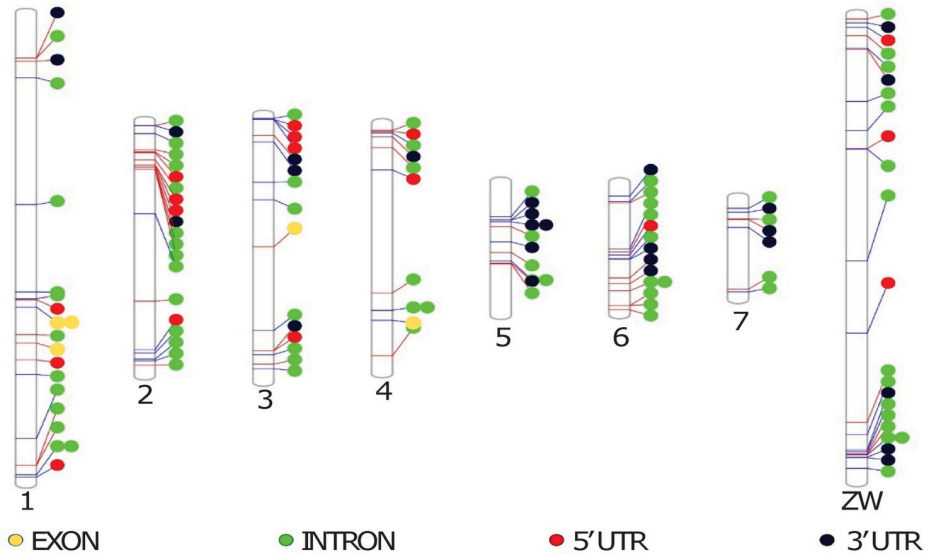
1
2
3
4
5
6
7
ZW
EXON
INTRON
5'UTR
3'UTR

Fig 3. Intragenic PQS distribution within the *S. mansoni* genome. A) The distribution of intragenic PQS per individual chromosomes. For each chromosome, intragenic PQS were categorised into those found within introns, exons, 5′- and 3′-UTRs. The largest number of PQS were found on chromosome ZW and the fewest on chromosome 7, with most PQS aligned to intronic features and fewest PQS found within exons. B) Intragenic PQS per Mb were calculated for each chromosomal feature and compared to the average intragenic PQS per Mb for all features (dotted horizontal line = baseline). Both 5′- and 3′- UTR categories had greater PQS per Mb than the calculated baseline (0.56). Multiple comparisons found 3′- UTRs were enriched with more PQS/mb compared to other features. C) Phenogram detailing localisation of intragenic PQS in each chromosome. Coloured circles denote PQS location according to intragenic feature.

https://doi.org/10.1371/journal.pntd.0008770.g003

stable conformations, either parallel or anti-parallel, we wanted to directly identify the presence of G4 epitopes within the parasite itself. Thus, BG4, a single chain variable fragment (scfv) antibody [48], capable of detecting both RNA and DNA G4 structures in human and *Plasmodium* cells [11, 49] was used (Fig 6).

In male and female worms, BG4 (G4 targeting antibody) signal co-localised with DAPI and was broadly distributed throughout all cell types found within anterior, posterior and midsection regions of both sexes. Loss of BG4 signal was observed when worms were incubated with DNase I prior to processing (Fig 7A), but not following RNase A incubation (Figs 7B and S4 Fig). As the RNAse A used in these experiments was active (S5 Fig), this data suggested that the vast majority (all) of detectable, adult worm G4 was found in DNA.

Discussion

While previous studies have explored the presence and function of G4s in protozoan parasites, similar investigations in multicellular pathogens (i.e. worms) have not been systematically conducted [13, 14]. As parasitic helminths remain a significant cause of plant, animal and human disease, new biological insight into how these pathogens regulate complex lifecycles would benefit the development of novel control strategies. Towards this aim, and as an exemplar of a biomedically significant parasitic helminth, we demonstrate that stable G4 structures are present within the *S. mansoni* genome. This finding identifies a previous unexplored area of schistosome biology that may catalyse the development of novel schistosomiasis treatment options and fuel investigations in other parasitic worm species.

Utilising *in silico* approaches involving complementary software tools (QP and G4h), G4 regions are found within both intra- and inter-genic regions of the *S. mansoni* genome (Figs 2 and 3). Although the abundance of G4s present relative to genome size is low, stringent parameters were enforced to increase detection of true positives; it is, thus, to be expected that more G4 folding sequences exist in the parasite than we have detected here. High-throughput analytical techniques including G4Seq and BG4 CHIP techniques detect a higher incidence of G4 structures compared to computational predictions in a variety of genomes [21, 50]. It is, therefore, highly feasible that the same is true for the *S. mansoni* genome. There are also widely reported instances within the literature on sequence based detection of non-classical G4 structures (e.g. bulge quadruplexes or loop errors/mutations) that are not detectable by QP and are limited in detection by G4h [51, 52]. Therefore, many non-classical G4 would be missed in our analyses and this will also contribute to a conservative initial estimate.

The high number of PQS located in intergenic regions compared to intragenic regions is largely due to the tandem telomeric repeat widely confirmed to adopt G4 folding [53–55]. A search for the 'TTAGGG' repeat (and its reverse complement to account for the reverse strand) motif within PQS found that a large majority of intergenic PQS to be telomeric, a trend found across all chromosomes but in particular chromosome 5 (S2 Table). This may simply be due to quality of sequence coverage of chromosome 5 in the current genome assembly compared to other chromosomes. Telomeric PQS comprising the majority of detected intergenic PQS has

A

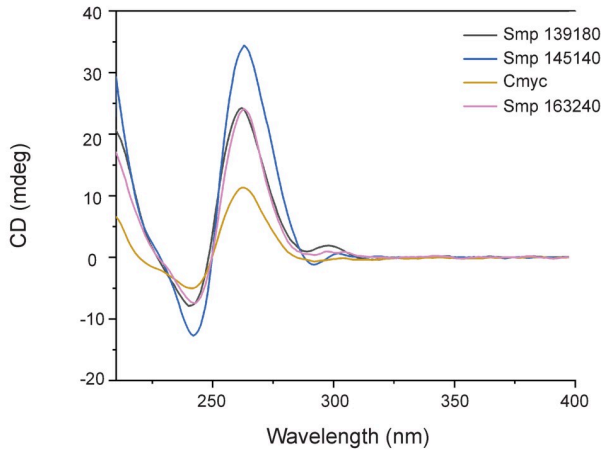
Smp 139180
Smp 145140
Cmyc
Smp 163240
CD (mdeg)
Wavelength (nm)
40
30
20
10
0
-10
-20
250
300
350
400

B

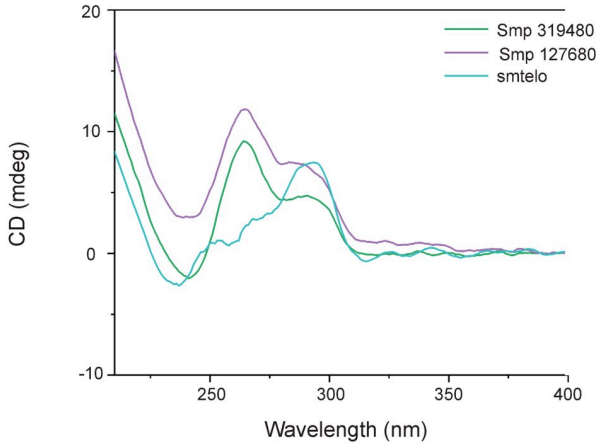
Smp 319480
Smp 127680
smtelo
CD (mdeg)
Wavelength (nm)
20
10
0
-10
250
300
350
400

C

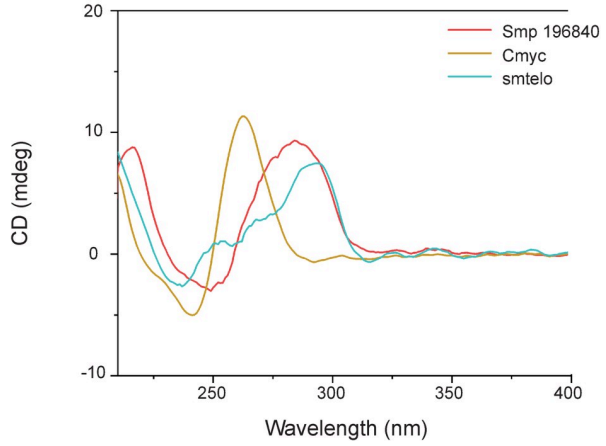
Smp 196840
Cmyc
smtelo
CD (mdeg)
Wavelength (nm)
20
10
0
-10
250
300
350
400

Fig 4. *In vitro* validation of *S. mansoni* oligonucleotides containing PQS by circular dichroism. Oligonucleotides containing predicted PQS within Smps were annealed in the presence of K^+ before cooling and recording spectra by circular dichroism. A) *smp_139180*, *smp_145140* and *smp_163240* compared to *c-myc* control, indicating a parallel G4 conformation. B) *smp_319480* and *smp_127680* in comparison to *smTelo* control, with spectra indicative of an anti-parallel hybrid quadruplex. C) *smp_196840* with both controls, indicating a spectra readout that does not correlate with either parallel or hybrid quadruplex formation.

https://doi.org/10.1371/journal.pntd.0008770.g004

been observed in *P. falciparum* and indeed many eukaryotes [14, 18, 21]. While non telomeric intergenic PQS have been observed across many species, research into their function is mostly limited to intragenic counterparts [11, 56, 57]. Non-telomeric intergenic PQS have been hypothesised to block transcription in *Arabidopsis* due to their proximity to transcription start sites, but this has not been explored greatly in other systems [57].

Although the range of intragenic PQS across chromosomes is fairly limited (7–23 PQS), chromosome 5 appears greatly enriched for PQS compared to all other chromosomes following normalisation (Fig 3). Chromosome 5 does not differ significantly in GC content compared to other chromosomes (Fig 2B) and indicates that PQS are not present due to an increase in GC content in the chromosome. The reason for increased numbers of PQS in this chromosome is currently unclear and requires further exploration.

The low absolute number of PQS detected within exons may, in part, be due to the phenomenon of large introns within the genome [2]. Indeed, the average length of an *S. mansoni* intron is 1,692 bp (with some up to 33.8 kb reported) compared to an average exon length of 217 bp and this likely accounts for a higher number of absolute intronic PQS compared to other intragenic motifs [2]. Upon normalisation, the intragenic PQS rate is scarce, but it is important to note that *S. mansoni* has a relatively large genome (397.2 Mb) with long stretches of noncoding areas and this trait is also observed in other AT rich genomes such as *Plasmodium* [3, 18]. Despite a high absolute number of intronic PQS, the greatest enrichment of PQS (when normalised to chromosomal feature) was detected in the 3′ regions, and then 5′ regions. Mammalian genomes (mouse and human) are also enriched for PQS within the 5′ region and especially in promoters [21], but in contrast do not feature the strong 3′ enrichment seen here in *S. mansoni*. Over-enrichment of PQS in 3′ UTRs has also been observed in the *Arabidopsis* genome, although the functionality of such motifs was not explored further [21]. G4s within mRNA 3′ UTRs are associated with cis-regulatory control mechanisms including translational repression and regulation of miRNA binding, with G4s masking miRNA binding sites and leading to shorter transcripts through modulation of polyadenylation efficiency [58, 59]. The *S. mansoni* genome encodes miRNAs with research suggesting an important role in parasite developmental biology, sexual maturation and host cell modulation [60–62]. G4s in 3′ UTRs may thus, potentially be associated with miRNA mediated gene expression regulation within the parasite, highlighting a future endeavour to be explored in further contextualising the functional role of *Schistosoma* G4.

GO term analysis revealed a significant enrichment of PQS within genes associated with the *wnt* signalling pathway (confirmed by CD for *smp_145140-wnt* and *smp_139180-frizzled*; Fig 4 and S3 Table), a crucial developmental system necessary for parasite development [63–65]. In the Platyhelminthes, *wnt* is associated with proper axial development and maintenance of anterior-posterior polarity [4, 65] and so targeting G4 present within *wnt*-associated genes may provide a potential avenue in disrupting parasite development. *S. mansoni* contains a *wnt* gene orthologous to planarian *wnt2* that is expressed in a spatial gradient along the worm posterior, suggesting linkage with axial development [4]. Within *S. japonicum*, both *wnt* (*Sjwnt4* and *Sjwnt5*) and *frizzled (Sjfz7*) genes have been identified and characterised across multiple lifecycle stages of the parasite [64, 66, 67]. *Sjwnt5* was additionally linked with reproductive

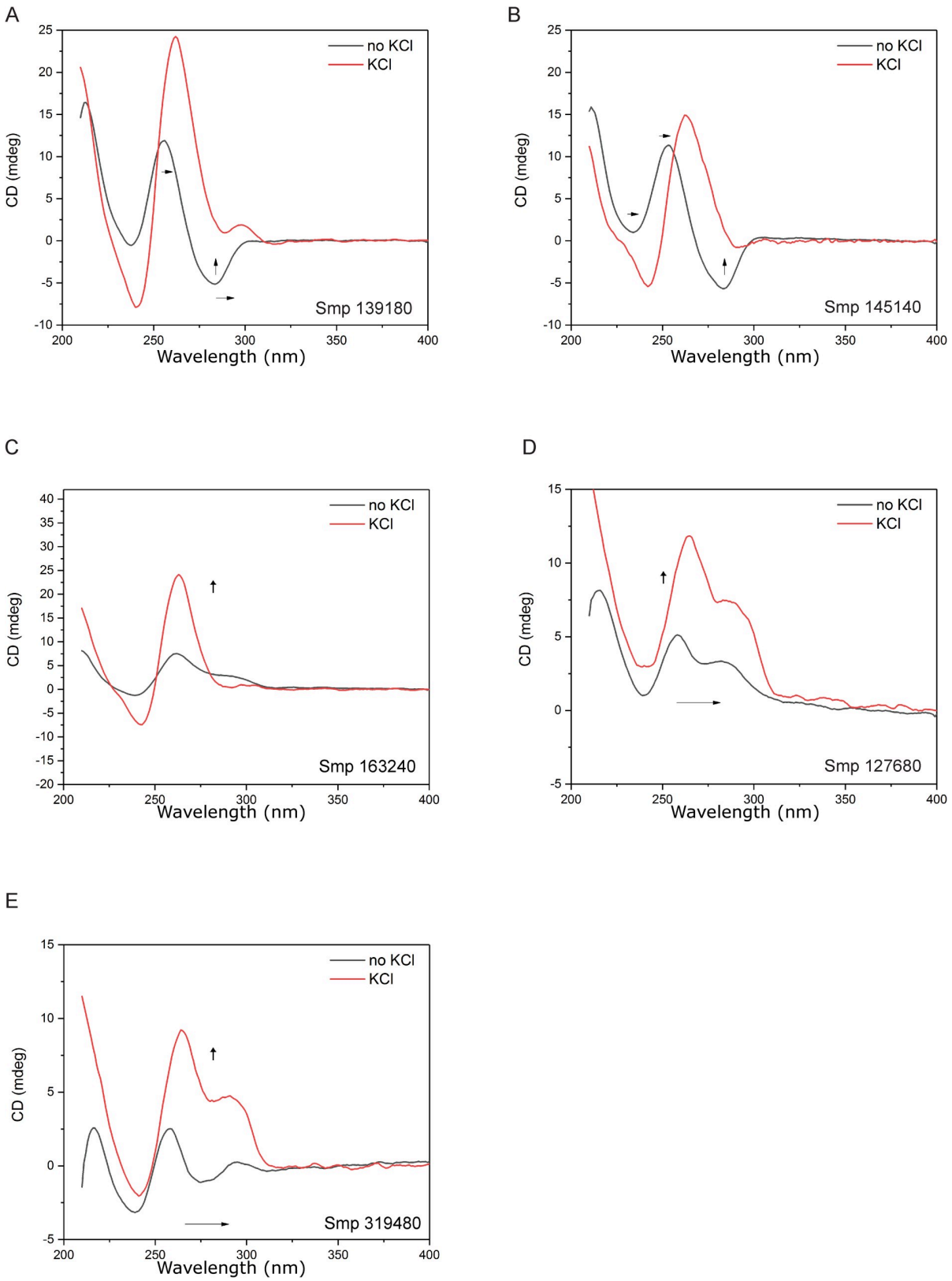

Fig 5. G4 stability of PQS-containing oligonucleotides is dependent on K^+. PQS containing oligos were annealed in the presence (red line) or absence (black line) of K^+ ions and spectra recorded for A) *smp_139180* B) *smp_145140* C) *smp_163240* D) *smp_127680* and E)

smp_319480. Addition of K^+ ions leads to spectral shifts towards higher wavelengths in all oligonucleotides and increased ellipticity can be observed in the presence of K^+.

https://doi.org/10.1371/journal.pntd.0008770.g005

organ development and is found highly expressed in testes, ovaries and vitellarium [65]. Interestingly, G4s have been identified in genes encoding components of the *wnt* pathway in other organisms. Specifically, G4s are found in the promoter region of human *wnt1* and this was found to be sensitive to G4 stabilising compounds [68]. Furthermore, G4s have also been described in both human and zebrafish *fzd5* where they have been associated with transcriptional control of the gene [69, 70]. Collectively, these findings suggest that G4 enrichment in genes encoding *wnt* pathway components is conserved across genomes and may have functional implications. The evolutionary importance of G4 can be further contextualised by analysis of other *Schistosoma* (and indeed, other platyhelminth) genomes for PQS. Retention of G4 sites within conserved genes could help further develop our understanding of this genomic feature within schistosome developmental biology. Further biological importance of PQS could be explored by considering haplotypic or sex associated genes.

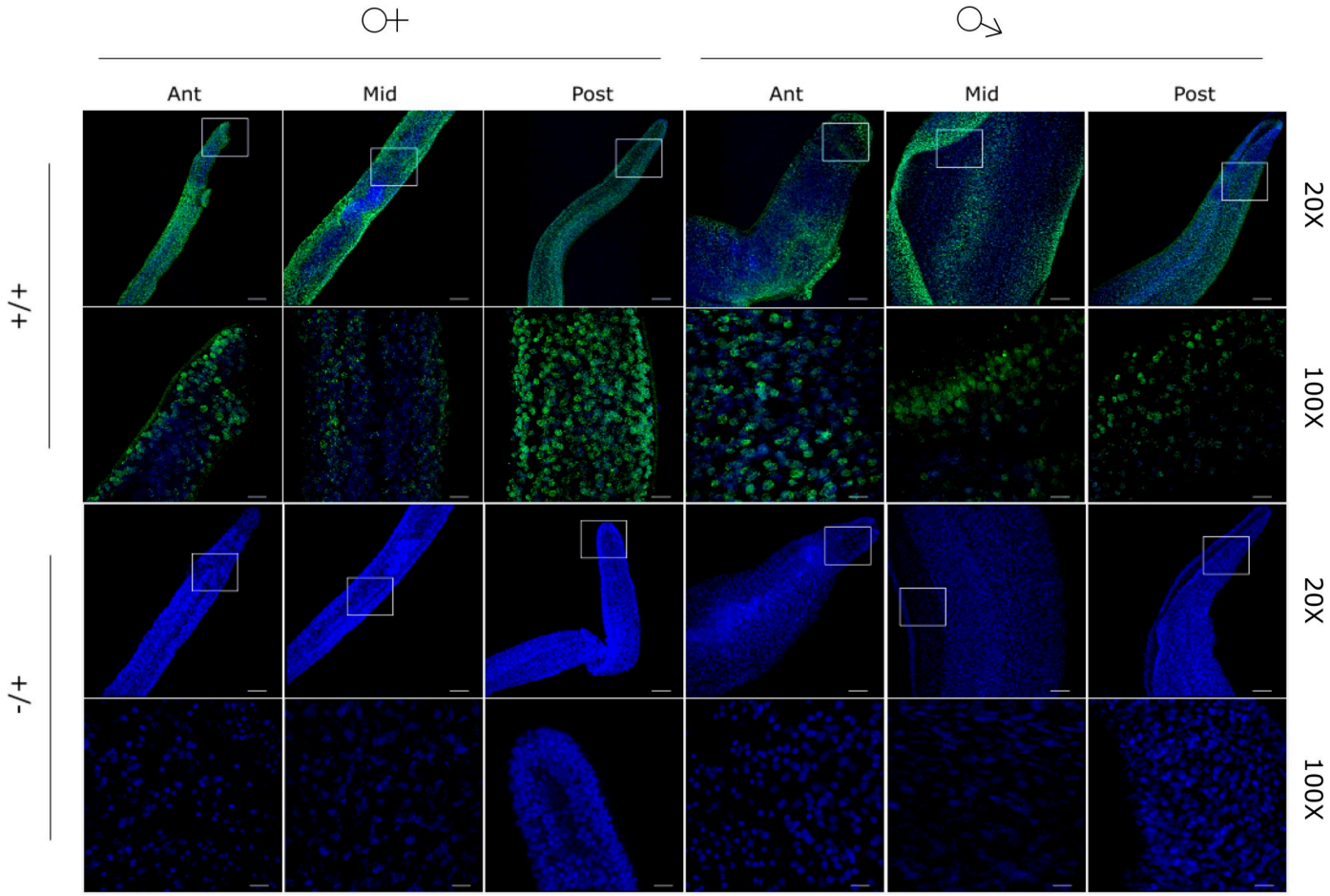

Fig 6. G4 structures are detectable in adult schistosomes. Male and female worms were stained with anti-quadruplex recognising BG4 (green) and counterstained with DAPI (blue). +/+ denotes the use of both primary and secondary antibodies, -/+ denotes the use of secondary antibody only (control). Z stacks of adult anterior (Ant), midsection (Mid) and posterior (Post) regions were taken using a Leica SP8 confocal microscope. Samples were imaged at 20X (scale bar = 50 μm) and then 100X, (scale bar = 10 μm), with box denoting region enlarged. Strong BG4 signal (488 nm) is co-localised with DAPI signal (405 nm) and is observed in both female and male samples.

https://doi.org/10.1371/journal.pntd.0008770.g006

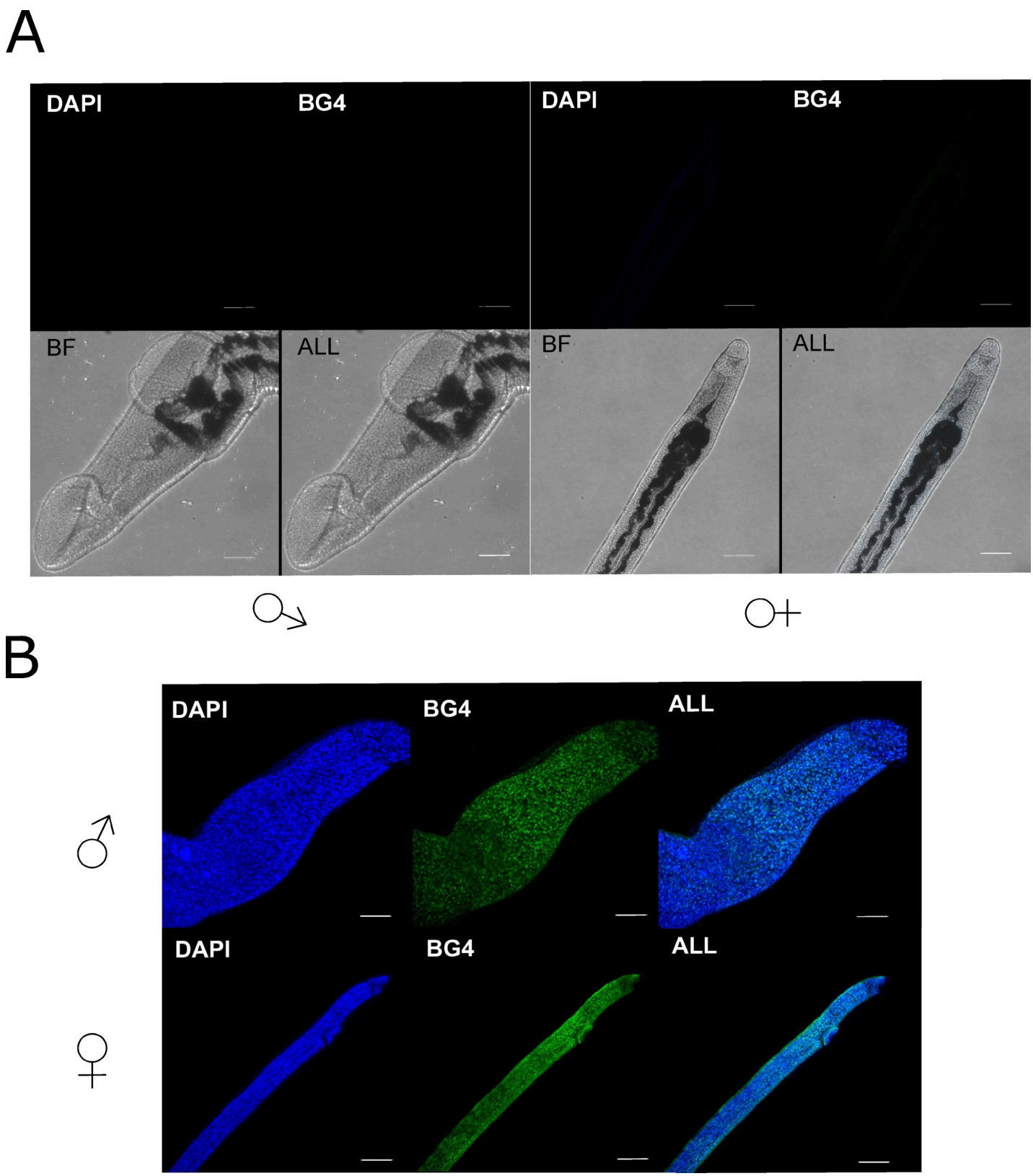

Fig 7. Adult schistosome G4 is predominantly found within DNA, and not RNA, pools. Schistosomes were either treated with A) 120 U DNase I or B) 0.1 mg/ml RNase A for 1 hr at 37˚C post permeabilisation and prior to blocking. Anterior sections from males and females were imaged using a Leica SP8 confocal microscope and

images collated from Z stacks. Samples were incubated with BG4 (481 nm) and counterstained with DAPI (405 nm) prior to visualisation. Brightfield images were taken for DNase I treated samples due to the absence of any fluorescent signal at either 481 nm (green channel) or 405 nm (blue channel). Scale bar denotes 10 μm.

https://doi.org/10.1371/journal.pntd.0008770.g007

CD spectra demonstrate that PQS within *S. mansoni* protein coding genes can fold unambiguously into higher order G4 structures when exposed to quadruplex favouring conditions (Fig 4). PQS-containing oligonucleotides representing *smp_139180*, *smp_163240* and *smp_145140* folded into structures with spectra comparable to the *H. sapiens c-myc* control, a known parallel G4. In contrast, PQS-containing oligonucleotides representing *smp_319480* and *smp_127680* displayed CD spectra that mirrored that of hybrid G4s found in *smTelo* as well as elsewhere [71–73], and showed a comparable stability. With respect to the parallel folded G4s, the high T_m observed for the oligonucleotide *smp_163240* and the impossibility to extrapolate a T_m for *smp_145140*, indicate thermodynamic stability associated with single nucleotide loop motifs (S3 Fig), which have been characterised in *H. sapiens vegf* and *c-kit*, as well as the *c-myc* control used in our study [74, 75]. Indeed, the only oligonucleotide representative to adopt a parallel folded G4 structure and to not contain a single nucleotide loop was derived from *smp_139180*; this oligonucleotide also demonstrated the lowest T_m among the three sequences.

Of note, the only PQS-containing oligonucleotide that did not resolve into a G4 structure was derived from *smp_196840*. Specifically, this oligonucleotide displayed CD spectra more commonly associated with B form DNA structures [76]. A possible explanation for the lack of classical G4-folding for this DNA sequence, when compared to the others, could be due to the length of the sequence; *smp_196840*'s oligonucleotide was the second longest (33 nt) and contained the longest loop length between G quartets (9 nt). Combined, these two factors may contribute to a greater instability of the oligo and a reduced likelihood of G4 formation, as shorter loop lengths are often associated with a more stable tertiary structure [77, 78]. This phenomenon is not unusual as other instances of computationally predicted PQS not folding *in vitro* have been reported [77].

The CD data also confirm that G4 folding is K^+ dependent (Fig 5). Cations are crucial for G4 formation and stability, contributing to G4 tetrad stabilisation by electrostatic binding to the O6 of the guanines and interacting with the negative charges of the phosphate backbone [79]. Although there is some higher order folding detectable in the *S. mansoni* G4 sequence in absence of monovalent cations (Fig 5), these are likely not G4-type structures, as indicated by the spectra and ellipticity. Therefore, K^+ is needed for G4 folding within *S. mansoni* derived PQS.

The immunofluorescent detection of G4 within adult worm nuclei ($DAPI^+$) clearly validates the *in silico* predictions/CD spectra confirmation of PQS within this parasitic worm (Fig 6). While the BG4 antibody can recognise G4 epitopes in both RNA and DNA [80, 81], the loss of signal when adult worms were treated with DNase I, but not RNaseA, strongly suggests that most G4s are found in the DNA pool (Fig 7). Within the nucleus, the location of the DNA-associated G4 cannot be specifically resolved by our current LSCM analyses. However, the transient nature of G4s and the abundance required for visualisation by this technique, it is likely that the signal observed here is derived from telomeric G4s given the large number detected in computational analyses (S2 Table). As this indicates that many PQS are present within the terminal ends of chromosomes (derived from the schistosomal telomeric tandem repeat TTAGGG) and this repeat can form a stable G4 structure (Fig 4) similar to *htelo* [82–85], this reasonably accounts for the signal seen. Telomerase has been shown to bind to telomeric G4 across organisms including humans and ciliates [86–89]; therefore, future IF co-localisation experiments with BG4 and anti-telomerase Abs could support this observation.

Additionally, detection of G4 in metaphase chromosomes could provide further information relevant to spatial PQS distribution in *S. mansoni*.

The presence of G4 could provide a new chemotherapeutic target for treating *S. mansoni* infection. Evidence to support this contention exists in parasitic protozoa where naphthalene diimide ligands that bind G4 within nuclei of kinetoplasts have shown anti-parasitic activity against *T. brucei* [12, 27]. Furthermore, G4 binding fluoroquinolones that disrupt G4 DNA-protein interactions and inhibit Pol I elongation [13, 90] have shown activity against *P. falciparum* and *T. brucei* with greater selectivity than human cells [11]. Indeed, the fluoroquinolone compound CX 3542 (Quarfloxin) has bioavailability within human erythrocytes, which could present an ideal delivery strategy for targeting *Schistosoma* and other haematophagous parasites [91]. Given the importance of transcriptional and translational control for survival of organisms (i.e. schistosomes) that have evolutionarily undergone gene loss as they become more parasitised, targeting G4 containing sequences could represent a novel anthelmintic strategy.

In summary, G4s were identified in the parasitic platyhelminth *S. mansoni* for the first time. Computational analysis suggests that G4s are distributed across all chromosomes with *in vitro* validation that putative G4-containing sequences can fold into stable PQS as visualised by CD spectroscopy. Confocal microscopy of adult schistosomes demonstrates the *in vivo* presence of G4s in fixed parasites. This lends credence to the presence of G4 as functional operators within the parasite and opens up previously unknown avenues for exploration in parasite biology, development and regulation.

Supporting information

S1 Fig. Example topographies of G4 structures. G4 have several topographical structures where strand directionality (arrowheads) and loop formation differ, affecting the tetrad each guanine forms (grey). A) In parallel G4 (e.g. *H. sapiens c-myc*), all four strands have the same directionality and loops form as "propellers" outwards from the stacked tetrads. B) In anti-parallel G4, strands have opposite directionality and loops form above as well as below the G4. C) In hybrid (3+1) G4, one strand runs anti-parallel to the rest and the loops are a mix of those found in parallel and anti-parallel G4 (e.g. *H. sapiens hTelo*).
(TIF)

S2 Fig. Structure of PQS containing oligonucleotides are differentially affected by temperature. Oligos were adjusted to a 6 μM working solution in 60 mM TrisKCl (10 mM TrisHCl, 50 mM KCl; pH 7.4) buffer. CD spectra were recorded at 5˚C intervals between 25˚C and 95˚C; data was used to calculate T_ms. Parallel forming oligonucleotide sequences A) *smp_139180*, B) *smp_145140* and C) *smp_163240* showed stable structures that lost some ellipticity but not completely. Hybrid G4 folding oligonucleotide sequences D) *smp_127689* followed the same trend as above whereas E) *smp_319480* totally lost its ellipticity as temperature increased, indicating a complete unfolding of the G4.
(TIF)

S3 Fig. Melt curves of thermodynamic stability analysis. Spectra was recorded by CD at 5˚C intervals between 95 and 25˚C. Normalised CD was plotted, and T_m determined for each oligo sequence. Three repeats (average reading shown) were performed for each temperature point and regression analysis was performed to fit curves.
(TIF)

S4 Fig. Treatment of adult worms with RNase A does not affect the detection of BG4 signal. Mean signal intensities were acquired from LSCM images of male and female worms

treated with enzymatically active RNase A (Fig 7) or buffer (enzyme free) controls (Fig 6). Mean intensity for each image were calculated by ImageJ and plotted as individual data points. Mean + SEM was plotted and Mann-Whitney t test was performed. No significance was observed between groups, indicating signal is not from RNA G4 structures.
(TIF)

S5 Fig. RNaseA is enzymatically active. A sample of 1 μg each of total murine RNA and *S. mansoni* RNA were incubated for 1 hr in 0.1 mg/ml RNase (37 ^{o}C) and electrophoresed on an agarose gel with a 1kB ladder alongside RNA only controls (incubated under the same conditions in the absence of RNaseA). Complete degradation of host/parasite RNA was only observed in the presence of RNaseA (R+).
(TIF)

S1 Table. Identification of PQS in the *S. mansoni* genome using QP and G4H. Sequences identified by each software algorithm are included as is the consensus sequence (those conserved sequences identified by both software).
(XLSX)

S2 Table. Number of telomeric and non-telomeric intergenic PQS per chromosome.
(DOCX)

S3 Table. Gene Ontology enrichment analysis of *S. mansoni* PQS.
(XLSX)

Acknowledgments

We acknowledge Ms Julie Hirst and all members of the Hoffmann laboratory for assistance in *Schistosoma* life cycle maintenance. We thank Dylan Phillips and Alan Cookson for advice on fluorescence imaging. Some *B. glabrata* snails used in this study were provided by the NIAID Schistosomiasis Resource Centre of the Biomedical Research Institute (Rockville, MD, USA) through NIH-NIAID Contract HHSN272201000005I for distribution through BEI Resources.

Author Contributions

Conceptualization: Holly M. Craven, Martin Swain, Helen Whiteland, Angela Casini, Karl F. Hoffmann.

Data curation: Holly M. Craven.

Formal analysis: Holly M. Craven, Riccardo Bonsignore, Vasilis Lenis, Daniel Berrar, Martin Swain, Helen Whiteland.

Funding acquisition: Helen Whiteland, Karl F. Hoffmann.

Investigation: Holly M. Craven, Riccardo Bonsignore, Nicolo Santi.

Methodology: Holly M. Craven.

Project administration: Angela Casini, Karl F. Hoffmann.

Resources: Angela Casini, Karl F. Hoffmann.

Software: Vasilis Lenis, Martin Swain.

Supervision: Martin Swain, Helen Whiteland, Karl F. Hoffmann.

Validation: Holly M. Craven, Riccardo Bonsignore.

Visualization: Holly M. Craven, Riccardo Bonsignore.

Writing – original draft: Holly M. Craven.

Writing – review & editing: Holly M. Craven, Helen Whiteland, Karl F. Hoffmann.

References

1. McManus DP, Dunne DW, Sacko M, Utzinger J, Vennervald BJ, Zhou X-N. Schistosomiasis. Nat Rev Dis Prim. 2018; 4: 13. https://doi.org/10.1038/s41572-018-0013-8 PMID: 30093684
2. Berriman M, Haas BJ, LoVerde PT, Wilson RA, Dillon GP, Cerqueira GC, et al. The genome of the blood fluke *Schistosoma mansoni*. Nature. 2009; 460: 352–U65. https://doi.org/10.1038/nature08160 PMID: 19606141
3. Protasio A V, Tsai IJ, Babbage A, Nichol S, Hunt M, Aslett MA, et al. A Systematically Improved High Quality Genome and Transcriptome of the Human Blood Fluke *Schistosoma mansoni*. PLoS Negl Trop Dis. 2012; 6. https://doi.org/10.1371/journal.pntd.0001455 PMID: 22253936
4. Wang J, Collins JJ. Identification of new markers for the *Schistosoma mansoni* vitelline lineage. Int J Parasitol. 2016; 46: 405–410. https://doi.org/10.1016/j.ijpara.2016.03.004 PMID: 27056273
5. Whiteland HL, Chakroborty A, Forde-Thomas JE, Crusco A, Cookson A, Hollinshead J, et al. An *Abies procera*-derived tetracyclic triterpene containing a steroid-like nucleus core and a lactone side chain attenuates in vitro survival of both *Fasciola hepatica* and *Schistosoma mansoni*. Int J Parasitol Drugs Drug Resist. 2018; 8: 465–474. https://doi.org/10.1016/j.ijpddr.2018.10.009 PMID: 30399512
6. Geyer KK, Rodríguez López CM, Chalmers IW, Munshi SE, Truscott M, Heald J, et al. Cytosine methylation regulates oviposition in the pathogenic blood fluke *Schistosoma mansoni*. Nat Commun. 2011;2. https://doi.org/10.1038/ncomms1433 PMID: 21829186
7. Wang J, Paz C, Padalino G, Coghlan A, Lu Z, Gradinaru I, et al. Large-scale RNAi screening uncovers therapeutic targets in the parasite *Schistosoma mansoni*. Science (80-). 2020; 369. https://doi.org/10.1126/science.abb7699 PMID: 32973031
8. Wendt G, Zhao L, Chen R, Liu C, O'Donoghue AJ, Caffrey CR, et al. A single-cell RNA-seq atlas of *Schistosoma mansoni* identifies a key regulator of blood feeding. Science (80-). 2020; 369: 1644–1649. https://doi.org/10.1126/science.abb7709 PMID: 32973030
9. Secor WE, Montgomery SP. Something old, something new: Is praziquantel enough for schistosomiasis control? Future Medicinal Chemistry. 1 Apr 2015 7: 681–684. https://doi.org/10.4155/fmc.15.9 PMID: 25996059
10. Tebeje BM, Harvie M, You H, Loukas A, McManus DP. Schistosomiasis vaccines: where do we stand? Parasites and Vectors. BioMed Central Ltd.; 2016. pp. 1–15. https://doi.org/10.1186/s13071-015-1291-6 PMID: 26728523
11. Harris LM, Monsell KR, Noulin F, Famodimu MT, Smargiasso N, Damblon C, et al. G-Quadruplex DNA Motifs in the Malaria Parasite *Plasmodium falciparum* and Their Potential as Novel Antimalarial Drug Targets. Antimicrob Agents Chemother. 2018;62. https://doi.org/10.1128/AAC.01828-17 PMID: 29311059
12. Zuffo M, Stucchi A, Campos-Salinas J, Cabello-Donayre M, Martínez-García M, Belmonte-Reche E, et al. Carbohydrate-naphthalene diimide conjugates as potential antiparasitic drugs: Synthesis, evaluation and structure-activity studies. Eur J Med Chem. 2019; 54–66. https://doi.org/10.1016/j.ejmech.2018.11.043 PMID: 30503943
13. Kerry LE, Pegg EE, Cameron DP, Budzak J, Poortinga G, Hannan KM, et al. Selective inhibition of RNA polymerase I transcription as a potential approach to treat African trypanosomiasis. PLoS Negl Trop Dis. 2017; 11. https://doi.org/10.1371/journal.pntd.0005432 PMID: 28263991
14. Harris LM, Merrick CJ. G-Quadruplexes in Pathogens: A Common Route to Virulence Control? Plos Pathog. 2015; 11. https://doi.org/10.1371/journal.ppat.1004562 PMID: 25654363
15. Gage HL, Merrick CJ. Conserved associations between G-quadruplex-forming DNA motifs and virulence gene families in malaria parasites. BMC Genomics. 2020; 21: 236. https://doi.org/10.1186/s12864-020-6625-x PMID: 32183702
16. Gazanion E, Lacroix L, Alberti P, Gurung P, Wein S, Cheng M, et al. Genome wide distribution of G-quadruplexes and their impact on gene expression in malaria parasites. Di Antonio M, editor. PLOS Genet. 2020; 16: e1008917. https://doi.org/10.1371/journal.pgen.1008917 PMID: 32628663
17. Rawal P, Kummarasetti VBR, Ravindran J, Kumar N, Halder K, Sharma R, et al. Genome-wide prediction of G4 DNA as regulatory motifs: Role in *Escherichia coli* global regulation. Genome Res. 2006; 16: 644–655. https://doi.org/10.1101/gr.4508806 PMID: 16651665

18. Smargiasso N, Gabelica VV, Damblon C, Rosu FF, De Pauw E, Teulade-Fichou M-PP, et al. Putative DNA G-quadruplex formation within the promoters of *Plasmodium falciparum* var genes. BMC Genomics. 2009; 10: 1–12. https://doi.org/10.1186/1471-2164-10-1 PMID: 19121221

19. Capra JA, Paeschke K, Singh M, Zakian VA. G-Quadruplex DNA Sequences Are Evolutionarily Conserved and Associated with Distinct Genomic Features in *Saccharomyces cerevisiae*. Plos Comput Biol. 2010;6. https://doi.org/10.1371/journal.pcbi.1000861 PMID: 20676380

20. Wolfe AL, Singh K, Zhong Y, Drewe P, Rajasekhar VK, Sanghvi VR, et al. Rudimentary G-quadruplex-based telomere capping in *Saccharomyces cerevisiae*. Nucleic Acids Res. 2009; 18: 764–7. https://doi.org/10.1038/nchem.1548.Quantitative

21. Marsico G, Chambers VS, Sahakyan AB, McCauley P, Boutell JM, Antonio M Di, et al. Whole genome experimental maps of DNA G-quadruplexes in multiple species. Nucleic Acids Res. 2019; 47: 3862–3874. https://doi.org/10.1093/nar/gkz179 PMID: 30892612

22. Siddiqui-Jain A, Grand CL, Bearss DJ, Hurley LH. Direct evidence for a G-quadruplex in a promoter region and its targeting with a small molecule to repress c-MYC transcription. Proc Natl Acad Sci U S A. 2002; 99: 11593–11598. https://doi.org/10.1073/pnas.182256799 PMID: 12195017

23. Qin Y, Hurley LH. Structures, folding patterns, and functions of intramolecular DNA G-quadruplexes found in eukaryotic promoter regions. Biochimie. 2008; 90: 1149–1171. https://doi.org/10.1016/j.biochi.2008.02.020 PMID: 18355457

24. Bidzinska J, Cimino-Reale G, Zaffaroni N, Folini M. G-Quadruplex Structures in the Human Genome as Novel Therapeutic Targets. Molecules. 2013; 18: 12368–12395. https://doi.org/10.3390/molecules181012368 PMID: 24108400

25. Lam EYN, Beraldi D, Tannahill D, Balasubramanian S. G-quadruplex structures are stable and detectable in human genomic DNA. Nat Commun. 2013;4. https://doi.org/10.1038/ncomms2792 PMID: 23653208

26. Rhodes D, Lipps HJ. Survey and summary G-quadruplexes and their regulatory roles in biology. Nucleic Acids Res. 2015; 43: 8627–8637. https://doi.org/10.1093/nar/gkv862 PMID: 26350216

27. Belmonte-Reche E, Martínez-García M, Guédin A, Zuffo M, Arévalo-Ruiz M, Doria F, et al. G-Quadruplex Identification in the Genome of Protozoan Parasites Points to Naphthalene Diimide Ligands as New Antiparasitic Agents. J Med Chem. 2018; 61: 1231–1240. https://doi.org/10.1021/acs.jmedchem.7b01672 PMID: 29323491

28. Gardner MJ, Hall N, Fung E, White O, Berriman M, Hyman RW, et al. Genome sequence of the human malaria parasite *Plasmodium falciparum*. Nature. 2002; 419: 498–511. https://doi.org/10.1038/nature01097 PMID: 12368864

29. Hirai H, LoVerde PT. Identification of the telomeres on *Schistosoma mansoni* chromosomes by FISH. J Parasitol. 1996/06/01. 1996; 82: 511–512. PMID: 8636864

30. *Schistosoma mansoni* v7. Available: ftp://ftp.sanger.ac.uk/pub/project/pathogens/Schistosoma/mansoni/v7/

31. Huppert JL, Balasubramanian S. Prevalence of quadruplexes in the human genome. Nucleic Acids Res. 2005; 33: 2908–16. https://doi.org/10.1093/nar/gki609 PMID: 15914667

32. Robinson JT, Thorvaldsdóttir H, Winckler W, Guttman M, Lander ES, Getz G, et al. Integrative genomics viewer. Nat Biotechnol. 2011; 29: 24–6. https://doi.org/10.1038/nbt.1754 PMID: 21221095

33. Bedrat A, Lacroix L, Mergny J-L. Re-evaluation of G-quadruplex propensity with G4Hunter. Nucleic Acids Res. 2016; 44: 1746–1759. https://doi.org/10.1093/nar/gkw006 PMID: 26792894

34. Quinlan AR, Hall IM. BEDTools: a flexible suite of utilities for comparing genomic features. Bioinformatics. 2010; 26: 841–842. https://doi.org/10.1093/bioinformatics/btq033 PMID: 20110278

35. Howe KL, Bolt BJ, Cain S, Chan J, Chen WJ, Davis P, et al. WormBase 2016: Expanding to enable helminth genomic research. Nucleic Acids Res. 2016; 44: D774–D780. https://doi.org/10.1093/nar/gkv1217 PMID: 26578572

36. Howe KL, Bolt BJ, Shafie M, Kersey P, Berriman M. WormBase ParaSite − a comprehensive resource for helminth genomics. Mol Biochem Parasitol. 2017; 215: 2–10. https://doi.org/10.1016/j.molbiopara.2016.11.005 PMID: 27899279

37. RStudio Team. RStudio: Integrated Development for R. Boston, MA; 2015. Available: http://www.rstudio.com

38. Holm S. A Simple Sequentially Rejective Multiple Test Procedure. Scand J Stat. 1979; 6: 65–70.

39. Klopfenstein D V., Zhang L, Pedersen BS, Ramírez F, Vesztrocy AW, Naldi A, et al. GOATOOLS: A Python library for Gene Ontology analyses. Sci Rep. 2018; 8. https://doi.org/10.1038/s41598-018-28948-z PMID: 30022098

40. Crusco A, Bordoni C, Chakroborty A, Whatley KCL, Whiteland H, Westwell AD, et al. Design, synthesis and anthelmintic activity of 7-keto-sempervirol analogues. Eur J Med Chem. 2018; 152: 87–100. https://doi.org/10.1016/j.ejmech.2018.04.032 PMID: 29698860

41. Smithers SR, Terry RJ. The infection of laboratory hosts with cercariae of *Schistosoma mansoni* and the recovery of the adult worms. Parasitology. 1965; 55: 695–700. https://doi.org/10.1017/s0031182000086248 PMID: 4957633

42. Hoffmann KF, Fitzpatrick JM. Gene expression studies using self-fabricated parasite cDNA microarrays. Methods Mol Biol. 2004; 270: 219–236. https://doi.org/10.1385/1-59259-793-9:219 PMID: 15153630

43. Karsisiotis AI, Hessari NMA, Novellino E, Spada GP, Randazzo A, Webba Da Silva M. Topological characterization of nucleic acid G-quadruplexes by UV absorption and circular dichroism. Angew Chemie—Int Ed. 2011; 50: 10645–10648. https://doi.org/10.1002/anie.201105193 PMID: 21928459

44. Del Villar-Guerra R, Gray RD, Chaires JB. Characterization of quadruplex DNA structure by circular dichroism. Curr Protoc Nucleic Acid Chem. 2017; 2017: 17.8.1–17.8.16. https://doi.org/10.1002/cpnc.23 PMID: 28252181

45. Mathad RI, Hatzakis E, Dai J, Yang D. C-MYC promoter G-quadruplex formed at the 5′-end of NHE III 1 element: Insights into biological relevance and parallel-stranded G-quadruplex stability. Nucleic Acids Res. 2011; 39: 9023–9033. https://doi.org/10.1093/nar/gkr612 PMID: 21795379

46. Wu G, Chen L, Liu W, Yang D. Molecular recognition of the hybrid-type G-quadruplexes in human telomeres. Molecules. 2019; 24. https://doi.org/10.3390/molecules24081578 PMID: 31013622

47. Carvalho J, Queiroz JA, Cruz C. Circular dichroism of G-Quadruplex: A laboratory experiment for the study of topology and ligand binding. J Chem Educ. 2017; 94: 1547–1551. https://doi.org/10.1021/acs.jchemed.7b00160

48. Biffi G, Tannahill D, McCafferty J, Balasubramanian S. Quantitative visualization of DNA G-quadruplex structures in human cells TL—5. Nat Chem. 2013; 5 VN-re: 182–186. https://doi.org/10.1038/nchem.1548 PMID: 23422559

49. Biffi G, Tannahill D, Miller J, Howat WJ, Balasubramanian S. Elevated levels of G-quadruplex formation in human stomach and liver cancer tissues. PLoS One. 2014; 9. https://doi.org/10.1371/journal.pone.0102711 PMID: 25033211

50. Chambers VS, Marsico G, Boutell JM, Di Antonio M, Smith GP, Balasubramanian S. High-throughput sequencing of DNA G-quadruplex structures in the human genome. Nat Biotechnol. 2015; 33: 877–+. https://doi.org/10.1038/nbt.3295 PMID: 26192317

51. Mukundan VT, Phan AT, Anh Tuan P. Bulges in G-Quadruplexes: Broadening the Definition of G-Quadruplex-Forming Sequences. J Am Chem Soc. 2013; 135: 5017–5028. https://doi.org/10.1021/ja310251r PMID: 23521617

52. Das K, Srivastava M, Raghavan SC. GNG motifs can replace a GGG stretch during G-quadruplex formation in a context dependent manner. PLoS One. 2016; 11. https://doi.org/10.1371/journal.pone.0158794 PMID: 27414642

53. Ambrus A, Chen D, Dai J, Bialis T, Jones RA, Yang D. Human telomeric sequence forms a hybrid-type intramolecular G-quadruplex structure with mixed parallel/antiparallel strands in potassium solution. Nucleic Acids Res. 2006; 34: 2723–2735. https://doi.org/10.1093/nar/gkl348 PMID: 16714449

54. Kolesnikova S, Curtis EA. Structure and Function of Multimeric G-Quadruplexes. Molecules. 2019; 24: 3074. https://doi.org/10.3390/molecules24173074 PMID: 31450559

55. Lin C, Yang D. Human telomeric G-quadruplex structures and G-quadruplex-interactive compounds. Methods in Molecular Biology. Humana Press Inc.; 2017. pp. 171–196. https://doi.org/10.1007/978-1-4939-6892-3_17 PMID: 28324509

56. Zizza P, Cingolani C, Artuso S, Salvati E, Rizzo A, D'Angelo C, et al. Intragenic G-quadruplex structure formed in the human CD133 and its biological and translational relevance. Nucleic Acids Res. 2016; 44: 1579–90. https://doi.org/10.1093/nar/gkv1122 PMID: 26511095

57. Mullen MA, Olson KJ, Dallaire P, Ois Major F, Assmann SM, Bevilacqua PC. RNA G-Quadruplexes in the model plant species *Arabidopsis thaliana*: prevalence and possible functional roles. https://doi.org/10.1093/nar/gkq804 PMID: 20860998

58. Rouleau S, Glouzon JPS, Brumwell A, Bisaillon M, Perreault JP. 3′ UTR G-quadruplexes regulate miRNA binding. RNA. 2017; 23: 1172–1179. https://doi.org/10.1261/rna.060962.117 PMID: 28473452

59. Beaudoin J-D, Perreault J-P. Exploring mRNA 3 0-UTR G-quadruplexes: evidence of roles in both alternative polyadenylation and mRNA shortening. https://doi.org/10.1093/nar/gkt265 PMID: 23609544

60. Zhu L, Liu J, Cheng G. Role of microRNAs in schistosomes and schistosomiasis. Frontiers in Cellular and Infection Microbiology. Frontiers Media S.A.; 2014. https://doi.org/10.3389/fcimb.2014.00165 PMID: 25426450

61. Simões MC, Lee J, Djikeng A, Cerqueira GC, Zerlotini A, da Silva-Pereira RA, et al. Identification of *Schistosoma mansoni* microRNAs. BMC Genomics. 2011; 12: 47. https://doi.org/10.1186/1471-2164-12-47 PMID: 21247453

62. Meningher T, Barsheshet Y, Ofir-Birin Y, Gold D, Brant B, Dekel E, et al. Schistosomal extracellular vesicle-enclosed miRNAs modulate host T helper cell differentiation. EMBO Rep. 2020; 21. https://doi.org/10.15252/embr.201947882 PMID: 31825165

63. Almuedo-Castillo M, Sureda-Gómez M, Adell T. Wnt signaling in planarians: New answers to old questions. International Journal of Developmental Biology. 2012. pp. 53–65. https://doi.org/10.1387/ijdb.113451ma PMID: 22450995

64. Li H-F, Wang X-B, Jin Y-P, Xia Y-X, Feng X-G, Yang J-M, et al. Wnt4, the first member of the Wnt family identified in *Schistosoma japonicum*, regulates worm development by the canonical pathway. Parasitol Res. 2010; 107: 795–805. https://doi.org/10.1007/s00436-010-1933-8 PMID: 20574838

65. Riddiford N, Olson PD. Wnt gene loss in flatworms. Dev Genes Evol. 2011; 221: 187–197. https://doi.org/10.1007/s00427-011-0370-8 PMID: 21892738

66. Ye Z, Xu J, Feng X, Jia Y, Fu Z, Hong Y, et al. Spatiotemporal expression pattern of Sjfz7 and its expression comparison with other frizzled family genes in developmental stages of *Schistosoma japonicum*. Gene Expr Patterns. 2019; 32: 44–52. https://doi.org/10.1016/j.gep.2019.02.005 PMID: 30851426

67. Ta N, Feng X, Deng LL, Fu Z, Hong Y, Liu J, et al. Characterization and expression analysis of Wnt5 in *Schistosoma japonicum* at different developmental stages. Parasitol Res. 2015; 114: 3261–3269. https://doi.org/10.1007/s00436-015-4545-5 PMID: 26077755

68. Chang LC, Chen TC, Chen SJ, Chen CL, Lee CC, Wu SH, et al. Identification of a new class of WNT1 inhibitor: Cancer cells migration, G-quadruplex stabilization and target validation. Oncotarget. 2016; 7: 67986–68001. https://doi.org/10.18632/oncotarget.6622 PMID: 27626678

69. Wang J-M, Huang F-C, Kuo MH-J, Wang Z-F, Tseng T-Y, Chang L-C, et al. Inhibition of cancer cell migration and invasion through suppressing the Wnt1-mediating signal pathway by G-quadruplex structure stabilizers. J Biol Chem. 2014; 289: 14612–23. https://doi.org/10.1074/jbc.M114.548230 PMID: 24713700

70. David AP, Margarit E, Domizi P, Banchio C, Armas P, Calcaterra NB. G-quadruplexes as novel cis-elements controlling transcription during embryonic development. Nucleic Acids Res. 2016; 44: 4163–4173. https://doi.org/10.1093/nar/gkw011 PMID: 26773060

71. Sagi J. G-quadruplexes incorporating modified constituents: A review. J Biomol Struct Dyn. 2014; 32: 477–511. https://doi.org/10.1080/07391102.2013.775074 PMID: 23528013

72. Vorlíčková M, Kejnovská I, Bednářová K, Renčiuk D, Kypr J. Circular dichroism spectroscopy of DNA: From duplexes to quadruplexes. Chirality. 2012. pp. 691–698. https://doi.org/10.1002/chir.22064 PMID: 22696273

73. Tariq Z, Barthwal R. Affinity of Anticancer Drug Daunomycin toward *Tetrahymena* Telomeric G-Quadruplex DNA D-[GGGG(TTGGGG) 3]. ACS Omega. 2019; 4: 6347–6359. https://doi.org/10.1021/acsomega.9b00331

74. Tippana R, Xiao W, Myong S. G-quadruplex conformation and dynamics are determined by loop length and sequence. Nucleic Acids Res. 2014; 42: 8106–8114. https://doi.org/10.1093/nar/gku464 PMID: 24920827

75. Chen Y, Yang D. Sequence, stability, and structure of G-Quadruplexes and their interactions with drugs. Curr Protoc Nucleic Acid Chem. 2012. https://doi.org/10.1002/0471142700.nc1705s50 PMID: 22956454

76. Kypr J, Kejnovská I, Renčiuk D, Vorlíčková M. Circular dichroism and conformational polymorphism of DNA. Nucleic Acids Research. 2009. pp. 1713–1725. https://doi.org/10.1093/nar/gkp026 PMID: 19190094

77. Guédin A, Gros J, Alberti P, Mergny JL. How long is too long? Effects of loop size on G-quadruplex stability. Nucleic Acids Res. 2010; 38: 7858–7868. https://doi.org/10.1093/nar/gkq639 PMID: 20660477

78. Lombardi EP, Londoño-Vallejo A, Nicolas A. Relationship between G-quadruplex sequence composition in viruses and their hosts. Molecules. 2019; 24. https://doi.org/10.3390/molecules24101942 PMID: 31137580

79. Bhattacharyya D, Arachchilage GM, Basu S. Metal cations in G-quadruplex folding and stability. Frontiers in Chemistry. Frontiers Media S. A; 2016. https://doi.org/10.3389/fchem.2016.00038 PMID: 27668212

80. Biffi G, Tannahill D, McCafferty J, Balasubramanian S. Quantitative visualization of DNA G-quadruplex structures in human cells. Nat Chem. 2013; 5: 182–186. https://doi.org/10.1038/nchem.1548 PMID: 23422559

81. Biffi G, Di Antonio M, Tannahill D, Balasubramanian S. Visualization and selective chemical targeting of RNA G-quadruplex structures in the cytoplasm of human cells. Nat Chem. 2014; 6: 75–80. https://doi.org/10.1038/nchem.1805 PMID: 24345950

82. De Cian A, Grellier P, Mouray E, Depoix D, Bertrand H, Monchaud D, et al. Plasmodium Telomeric Sequences: Structure, Stability and Quadruplex Targeting by Small Compounds. Chembiochem. 2008; 9: 2730–2739. https://doi.org/10.1002/cbic.200800330 PMID: 18924216

83. Wang Z-F, Chang T-C. Molecular engineering of G-quadruplex ligands based on solvent effect of polyethylene glycol. Nucleic Acids Res. 2012; 40: 8711–20. https://doi.org/10.1093/nar/gks578 PMID: 22735707

84. Parkinson GN, Lee MPH, Neidle S. Crystal structure of parallel quadruplexes from human telomeric DNA. Nature. 2002; 417: 876–880. https://doi.org/10.1038/nature755 PMID: 12050675

85. Wragg D, de Almeida A, Bonsignore R, Kühn FE, Leoni S, Casini A. On the Mechanism of Gold/NHC Compounds Binding to DNA G-Quadruplexes: Combined Metadynamics and Biophysical Methods. Angew Chemie—Int Ed. 2018; 57: 14524–14528. https://doi.org/10.1002/anie.201805727 PMID: 29972613

86. Moye AL, Porter KC, Cohen SB, Phan T, Zyner KG, Sasaki N, et al. Telomeric G-quadruplexes are a substrate and site of localization for human telomerase. Nat Commun. 2015; 6. https://doi.org/10.1038/ncomms8643 PMID: 26158869

87. Paudel BP, Moye AL, Assi HA, El-Khoury R, Cohen SB, Holien JK, et al. A mechanism for the extension and unfolding of parallel telomeric g-quadruplexes by human telomerase at single-molecule resolution. Elife. 2020; 9: 1–9. https://doi.org/10.7554/eLife.56428 PMID: 32723475

88. Oganesian L, Moon IK, Bryan TM, Jarstfer MB. Extension of G-quadruplex DNA by ciliate telomerase. EMBO J. 2006; 25: 1148–1159. https://doi.org/10.1038/sj.emboj.7601006 PMID: 16511573

89. Gomez D, Lemarteleur T, Lacroix L, Mailliet P, Mergny J-L, Riou J-F. Telomerase downregulation induced by the G-quadruplex ligand 12459 in A549 cells is mediated by hTERT RNA alternative splicing. Nucleic Acids Res. 2004; 32: 371–9. https://doi.org/10.1093/nar/gkh181 PMID: 14729921

90. Drygin D, Whitten JP, Rice WG, O'Brien S, Schwaebe M, Lin A, et al. Quarfloxin (CX-3543) disrupts the Nucleolin rDNA quadruplex complexes, inhibits the elongation by RNA Polymerase I and exhibits potent antitumor activity in models of cancer. Proc Am Assoc Cancer Res Annu Meet. 2008; 49: 784.

91. Papadopoulos K, Mita A, Ricart A, Hufnagel D, Northfelt D, Von Hoff D, et al. Pharmacokinetic findings from the phase I study of Quarfloxin (CX-3543): a protein-rDNA quadruplex inhibitor, in patients with advanced solid tumors. Mol Cancer Ther. 2007; 6.